Droplet Spectra Broadening by Ripening Process. Part I: Roles of Curvature and Salinity of Cloud Droplets

FIKRETTIN ÇELIK AND JOHN D. MARWITZ

Department of Atmospheric Science, University of Wyoming, Laramie, Wyoming

(Manuscript received 17 October 1997, in final form 11 August 1998)

ABSTRACT

The ''ripening process'' occurs due to thermodynamic instability of droplet size spectra in clouds. This instability results from the existence of droplets with different salinity and size in the droplet spectra. The ripening process is independent of turbulent fluctuations of supersaturation for a closed cloud parcel. Because of the ripening process, droplet number concentration continuously decreases with time after the initial peak supersaturation, which occurs during the initial updraft. Droplet spectra broaden to large sizes by evaporation of small droplets. Both mean droplet size and the standard deviation of droplet size spectra increase with time. This mechanism is suggested to be a potential physical mechanism for the formation of droplet size spectra in stratiform clouds.

1. Introduction

Cloud droplets with diameter >35 μm are required for the initiation of collision–coalescence instability for the generation of drizzle and rain in warm clouds (e.g., Klett and Davis 1973). Observational studies show that cloud droplet spectra are usually broad and sometimes bimodal (e.g., Warner 1969a). A large number of studies have been performed to explain droplet spectra broadening and formation of large droplets. A group of studies was related to the existence of giant aerosol particles (e.g., Woodcock 1950, 1952; Johnson 1976). Another group of studies was related to mixing processes. Mason and Jonas (1974) and Jonas and Mason (1982) developed a model of droplet spectra broadening by the mixing of successive thermals for cumulus clouds. In this model a cumulus cloud grows by ascent of successive thermals through the residues of their predecessors (multithermal model). Baker and Latham (1979) and Baker et al. (1980) considered inhomogeneous mixing of dry air with cloud. Telford and Chai (1980) proposed a model of mixing known as entity entrainment process. Another group of studies was connected to stochastic turbulent processes in clouds (Levin and Sedunov 1968; Sedunov 1965; Paluch 1971; Cooper 1989; among others).

A series of theoretical studies were related to the formation of droplet size spectrum in adiabatic isolated cloud parcels (e.g., Howell 1949; Squires 1952; Mason and Ghosh 1957; Mordy 1959; Neiburger and Chien 1960; among others). The major results from the early studies are summarized as follows. 1) Supersaturation reaches a maximum within a few decameters above cloud base; the activated particles grow and form cloud. 2) The main characteristics of the droplet spectrum are primarily defined by vertical velocity during the initial stage of formation of cloud. Because of the faster radial growth of small droplets than the growth of large droplets, a narrow unimodal droplet spectrum forms. 3) The existence of sufficient numbers of giant cloud condensation nuclei (CCN) is sufficient for the formation of large droplets to initiate collision–coalescence instability for precipitation formation in warm clouds. Warner (1969b) and Harding (1977) examined the effects of turbulence in the updraft velocity on the droplet size distribution in cumulus clouds. Warner (1969b) used a Lagrangian model for the evolution of droplet size spectra under random walk motions in a cloud. He concluded that turbulence in the updrafts does not broaden droplet spectra remarkably beyond that produced in a steady updraft. He also reported that certain structures of updrafts in a cloud can result in activation of fresh CCN to form broad bimodal droplet spectra. Hudson and Yum (1997) criticized the theoretical predictions of droplet spectra during adiabatic updraft of an individual parcel. They argued that adiabatic parcel models predict a decrease in the standard deviation of droplet sizes (σ_d) while the mean droplet size ($\overline{D}$) increases. On the other hand Hudson and Yum (1997) observed positive correlations between σ_d and $\overline{D}$ from airborne measurements. Cooper (1989), Hudson and Svensson (1995),

Corresponding author address: Dr. Fikrettin Çelik, Enviro-Meteo Services Inc., 135-8735 165th Street, Edmonton, AB T5R 2RG, Canada.

and Hudson and Yum (1997) argued that due to turbulence at the activation stage of cloud there will be variability in droplet size spectra in different parcels in a cloud. Mixing of these spectra from different locations of cloud can result in broadening of droplet size spectra. Kornfeld (1970) performed a series of numerical simulations on the formation of droplet spectra during updrafts with a few classes of CCN. It was concluded that the existence of soluble and insoluble CCN broadens droplet spectra. Hagen (1979) conducted numerical simulations to support cloud chamber laboratory experiments. In his simulation, temperature was decreased for the formation of cloud for 30 s (equivalent to lifting an air parcel). Then, by setting the temperature constant (nearly equivalent to setting vertical velocity equal to zero) for 16 min he observed the droplet spectra to broaden. In Hagen's simulation the diameter of the largest CCN was about 0.4 μm. The diameter of the largest size class of droplets was observed to increase a few microns during the 16 min of simulation. Hagen refered to the process as ''Ostwald ripening.'' Srivastava (1991) numerically simulated the evolution of 120 size classes of CCN in updraft with various magnitudes. The simulations were run until the Lagrangian parcels reached 3 km. He reported that the variance of the square of radius of droplet size distribution increases during updraft in the slow updraft cases. Recently, Korolev (1995) performed Lagrangian-based numerical simulations on the influence of turbulent fluctuations on the formation of droplet spectra. He concluded that fluctuations of the supersaturation arising from turbulent fluctuations broaden the droplet spectra.

Most of the previous studies were on cumuliform clouds. The problem of broadening of droplet spectra and the formation of large droplets for the onset of collision–coalescence processes is an important and active research area in cloud physics [see the review article of Beard and Ochs (1993) and the textbooks of Cotton and Anthes (1989) and Rogers and Yau (1989)].

In this study, a mechanism of droplet spectra broadening is introduced for stratiform clouds. The description of the mechanism is as follows. A cloud droplet size spectrum contains droplets with different size caused by different salinity. Small droplets have higher equilibrium supersaturation (s^*) than the s^* for larger droplets. Large droplets use the ambient supersaturation (s) to grow, thereby decreasing the s below the s^* for small droplets, thereby causing them to evaporate. Even if $s > s^*$ for some of the small droplets, some small droplets will not grow as fast as large ones. Thus, a narrow droplet size spectrum will broaden to large and small sizes. However, due to evaporation of small droplets this process will eventually narrow the droplet size spectrum. In the limit, the droplet size spectrum will contain droplets with uniform salinity and size (unisize spectrum). Thus, this process is a broadening process during the early stage (a few hours or longer); thereafter, it tends to be a narrowing process. This is an irreversible process of redistribution of liquid water among droplets or particles. In this mechanism, the s is maintained by evaporation of small droplets and growth of large droplets, which is different from the conventional condensational growth mechanism where s is maintained by updraft. This mechanism has similarity with droplet/particle growth by Ostwald ripening in colloid science (Everett 1988). Therefore, in this study this mechanism is called ''ripening process.'' In this paper, it is shown that the ripening process occurs in clouds and is an important mechanism for the formation of droplet size spectra for stratiform clouds.

Section 2 contains a description of the cloud model and initial conditions for numerical studies. Section 3 contains results from numerical simulations. Section 4 contains discussions and comparison with other studies and section 5 contains conclusions.

2. Mathematical model

a. Cloud model

The only requirement for the occurrence of the ripening process is the existence of droplets with different s^*. To show the role of the ripening process in a cloud a Lagrangian cloud model is used. The evolution of droplet spectra is simulated considering only the condensation process. Mixing between parcel and surroundings, gravitational fall of droplets, collision and coalescence processes, and ice phase processes are excluded. Thus, the cloud model is a closed, reversible adiabatic system. The evolution of droplet spectra is simulated by solving the basic cloud physics equations, which are given in appendix A. The validity of the model equations and numerical method for solution of the equations are discussed in appendix A.

b. CCN spectrum and initial conditions

A continental model aerosol spectrum is assumed. Aerosol measurements of Hobbs et al. (1985a) over the High Plains in the United States were taken as the representative aerosol spectrum. The model aerosol spectrum (Fig. 1a) was obtained by extrapolation from 0.02 to 1.2 μm from Fig. 6 of Hobbs et al. (1985a).

The model aerosol spectrum (Fig. 1a) contains water soluble and water insoluble dry particles. The water soluble particles act as CCN and they activate to form cloud droplets if the s exceeds the critical supersaturation (S_c). Activity spectrum (number of particles per unit volume that are activated to become cloud droplets) is expressed as a function of supersaturation. The relation between activity spectrum and supersaturation is given by the power law

$$N = Cs^k, \tag{1}$$

where N is the droplet number concentration at supersaturation s (%), C the droplet number concentration at

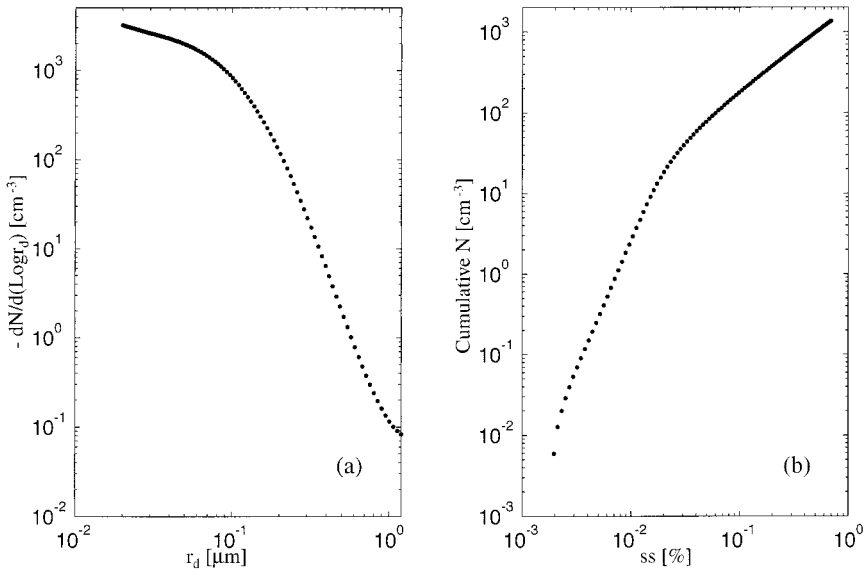

FIG. 1. (a) Model aerosol spectrum and (b) activity spectrum.

$s = 1\%$, and k the nondimensional empirical regression parameter (slope parameter). Activity spectrum was calculated using $C = 2000$ cm^{-3} and $k = 1.0$ (Fig. 1b). These values of C and k are consistent with the observational studies of Hobbs et al. (1985b) over the High Plains in the United States. The power-law relation with $C = 2000$ cm^{-3} and $k = 1.0$ estimates larger concentrations of CCN than the actual aerosol concentrations for $s < 0.04\%$. Therefore, the part of the activity spectrum with $s < 0.04\%$ is directly obtained from the aerosol spectrum (Fig. 1a). The slope parameter (k) in the region $s < 0.04\%$ has a value about 1.35. This value of k is comparable to the measurements of CCN at low s over the upwind side of Denver (Frisbie and Hudson 1993). The resulting activity spectrum is plotted in Fig. 1b. It was assumed that each CCN particle consisted of 80% $(NH_4)_2SO_4$ as water soluble and 20% as water insoluble material. The density of the dry CCN particles (ρ_d) was assumed to be 1.76 g cm^{-3} (Pruppacher and Klett 1978). The air parcel was specified to contain 100 CCN size classes. The CCN particles in each size class have the same chemical and physical characteristics.

The initial temperature (T), pressure (p), and relative humidity were assumed to be 270 K, 750 mb, and 98%, respectively. The equilibrium sizes of the haze particles at the initial relative humidity were calculated before starting the simulations. The condensation coefficient (β) and the thermal accommodation coefficient (α) were assumed to be 0.036 and 0.96, respectively.

3. Numerical simulations

a. Roles of salinity and curvature of droplets on the ripening process

Salinity and curvature of cloud droplets or haze particles are two important factors that determine the microphysical processes in cloud. The droplet growth equation, Eq. (A3) in the appendix can be rewritten as $dr/dt = (s - s^*)\Psi/r$. It is seen that the growth or evaporation of a droplet is determined by the relative difference between the s and s^* of a haze particle or cloud droplet. For a given s, droplets with $s^* < s$ will grow, droplets with $s^* > s$ will evaporate, and droplets with $s^* = s$ will be in equilibrium in size. The equation for s^*, which is given in the appendix, is rewritten herein as

$$s^* = \exp\left(\frac{2\sigma}{\rho_l R_v T r}\right)\left(1 + \frac{i\varepsilon M_w \rho_d r_d^3}{M_s(\rho' r^3 - \rho_d r_d^3)}\right)^{-1} - 1.$$

The exponential part of the above equation is due to the curvature effect. The curvature effect exponentially increases with decreasing droplet size. An increase in salinity (increase in size or ρ_d) tends to decrease s^*. Small size and/or low salinity of droplets produces higher s^*. The rate of growth or evaporation of a droplet is proportional to the difference between the s and s^*. The critical (or activation) supersaturation (S_c) is the supersaturation that corresponds to the critical (or activation) size of haze particles (r_c). Regardless of the fact that the radial growth or evaporation rate is inversely proportional to the size of the droplets, for a given s large droplets may grow faster than small droplets or large droplets may grow while small droplets may evaporate. The differences in growth or evaporation rates will be significantly greater among unactivated growing hygroscopic haze particles with large activation size and activated small droplets. The differences in the s^* of the droplets and particles in a given droplet spectrum are the driving force for the ripening process.

In the previous studies the salinity and curvature effects are generally considered in the evolution of cloud droplet size spectra during updrafts (i.e., activation and

growth of cloud droplets by adiabatic cooling). Based on numerical studies it is generally accepted that during updraft narrow droplet size spectra will form. The salinity and curvature terms are often neglected after the initial droplet size distribution that is determined during updraft or they are not considered in simulations by assuming an initial droplet size distribution. In these treatments, $dr/dt \propto s/r$. After the initial updraft stage s decreases to zero in a short time in the absence of external source of s (for a closed cloud parcel with the assumption that $dr/dt = s\Psi/r$). In this case, the droplet size spectrum is stable ($dr/dt = 0$) and there are no interactions among droplets.

To show the roles of salinity and curvature terms on the formation of droplet size spectra, evolution of droplet size spectrum in a given parcel was numerically simulated during updraft and for the rest of the cloud life up to 3 h. The largest dry CCN size was assumed to be 1 μm in radius.

The vertical velocity profile in this simulation is given as

$$w(t) = \begin{cases} w_o - \dfrac{w_o^2}{2H}t & t < t_H \\ 0 & t_H \le t \le 3h, \end{cases} \quad (2)$$

where $H = 200$ m, $w_o = 0.3$ m s^{-1}, and $t_H = 2H/w_o$ ($\sim$0.37 h). Therefore, the average vertical velocity is 0.15 m s^{-1} during updraft. (Note that stratiform clouds may have updraft velocities from 0.01 to 0.5 m s^{-1}. For example, during a synoptic-scale motion it can be very slow; on the other hand, during upslope motion over a mountain it can be on the order of 0.5 m s^{-1} or more). From 0 to 0.37 h, the air parcel moves 200 m upward, and from 0.37 to 3 h the parcel is stationary ($w = 0$). From 0 to 0.37 h is the updraft stage. During this stage, the s is mainly determined by adiabatic cooling due to updraft. This stage of cloud has been simulated by many other authors. However, from 0.37 to 3 h the parcel is at steady state ($w = 0$); that is, there is no source of s from adiabatic cooling.

In the absence of the ripening process (absence of curvature and salinity terms), using Eqs. (A3), (A4), and (A6) in the appendix, the ambient supersaturation for a steady-state cloud parcel ($w = 0$) with droplet concentration of N and integral average droplet diameter of $\overline{D}$ can be given as $ds/dt \cong -A(dX_w/dt)$, where $dX_w/dt = \pi\rho_l N\overline{D}s\Psi/m_d$ is the equation for liquid water mixing ratio, ρ_l is the density of water, and m_d is mass of dry air in the system [for a unit volume of air $m_d = \rho$ (density of dry air)]. Values of A and Ψ are around 431 and 5 $\times 10^{-11}$ m^2 s^{-1}, respectively, at $T = 270$ K and $p = 75\,000$ Pa. Thus, $ds/dt = -Bs$ and $s(t) = s_o \exp(-Bt)$, where $B = \pi\rho_l N\overline{D}\Psi A/m_d$. The characteristic time of s is $1/B$ s, which is around 7 s for $N = 100$ cm^{-3} and $\overline{D} = 20$ μm. Therefore, without the ripening process, the initial s left over from the updraft stage would be used up in less than 10 s.

In the absence of the ripening process, the increase in size of droplets due to use of s, which is left over from the updraft can be estimated analytically. For example, let us assume that the s has a value, s_h, just after the updraft. Using the definition of supersaturation and the relation between water vapor pressure and liquid water mixing ratio, the increase in liquid water mixing ration (ΔX_m) due to the use of s_h (drop of s from s_h to zero) would be $\Delta X_w \cong (\varepsilon/p)s_h e_s$ (note that $e - e_s = s_h e_s$) where $\varepsilon = 0.622$, p is air pressure, e and e_s are the water vapor pressure and saturation water vapor pressure, respectively. The corresponding increase in liquid water for a unit volume of cloud would be $\Delta L = \Delta X_w \rho$. If we assume a cloud parcel with N droplets per unit volume with an average diameter of $\overline{D}$ the increase in the size of the droplets (ΔD) due to the use of s_h would be

$$\Delta D = \left(\frac{6\Delta L}{\pi\rho_l N} + \overline{D}\right)^{1/3} - \overline{D},$$

where ρ_l is the density of water. For $s_h = 0.001$ (0.1%), $T = 270$ K, $p = 75\,000$ Pa, $N = 100$ cm^{-3}, and $\overline{D} = 20$ μm, the increase in the size of the droplets due to the decrease of s from s_h to zero is about $\Delta D = 0.06$ μm. This increase is negligible.

The results are shown in Fig. 2.[1] In this plot, the sizes of droplets in each class are plotted as a function of time. Therefore, each line corresponds to a class. The curvature term imposes a barrier for haze particles to activate. Thus, not all the haze particles grow or activate. The strong curvature effect of small droplets increases the rate of evaporation of smaller droplets, thus it causes broadening toward smaller sizes. At the same time, broadening toward smaller sizes increases the rate of release of water vapor, which is the source of s for the larger droplets to grow. Therefore, stronger curvature effects of smaller droplets causes growth of large droplets.

The droplet spectra at 0.5, 1, 2, and 3 h are plotted in Fig. 3 in terms of concentration as a function of size. This plot was generated from the simulation output by calculating concentrations of droplets at defined diameters $D_j = [4, 6, 8, \ldots, 46]$ μm:

$$N_j = \frac{1}{D_j^3}\sum_i N_i D_i^3, \qquad \{D_j - 1 \le D_i < D_j + 1\}, \quad (3)$$

where D_i and N_i are the diameters and concentrations of droplets with diameters in the region from $D_j - 1$ to $D_j + 1$, respectively. A narrow droplet spectrum was present at $t = 0.5$ h with more droplets at smaller sizes. The number concentration was decreasing at smaller

[1] Note that the presentation of the results is similar to the presentation of the results by other authors (e.g., Howell 1949; Mordy 1959; Srivastava 1991). The only difference is that the present results are plotted size as a function of time in linear scales.

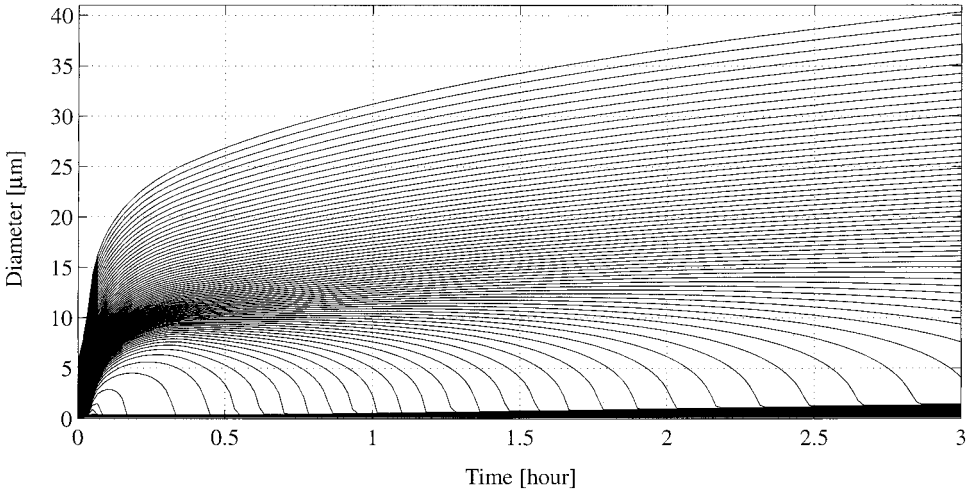

FIG. 2. Evolution of droplet size spectrum. Each line corresponds to time variations of droplet sizes in each class.

sizes while the spectrum was broadening toward larger sizes with time. The size of the peak in the spectrum increases with time.

Particles with $S_c >$ peak s during updraft will not activate. Some of the activated particles will deactivate if the s becomes less than s^* of the particles. Some of the activated particles grow during and after the updraft. The critical sizes of some particles may be very small ($\sim$1 μm). However, some hygroscopic particles with large critical (or activation) size will grow during and after the initial updraft before and after reaching their critical sizes. These particles may involve initiation of collision–coalescence processes before reaching their critical sizes (i.e., before becoming cloud droplets). In terms of initiation of warm rain, climate processes, and aircraft icing, classification of particles or droplets by size is more important than the classification of particles as activated or inactivated. For example, an unactivated haze particle 30 μm in diameter will be more important than an activated cloud droplet 2 μm in diameter. For airborne measurements of cloud droplet spectra, droplet concentration is done by classification of droplets or particles by size rather than classification by activated or unactivated particles. Therefore, in this study the particles or droplets larger than 2.4 μm in diameter are assumed to be a part of cloud droplet size spectra. Thus, droplet concentration and statistical parameters of droplet size spectrum are calculated for all droplets >2.4 μm in diameter.

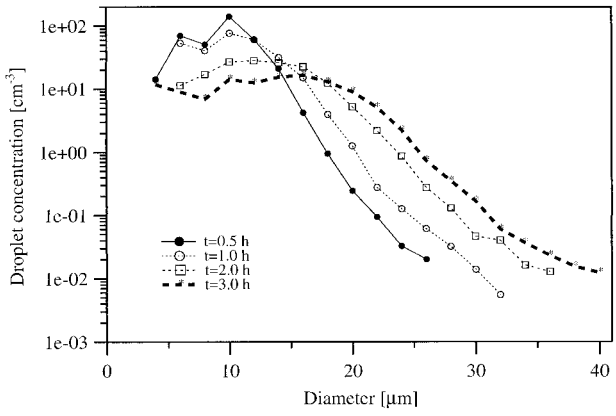

FIG. 3. Droplet spectra at 0.5, 1.0, 2.0, and 3 h for the simulation in Fig. 2.

Variations of the basic statistical parameters of droplet spectrum were calculated for simulation in Fig. 2. Mean diameter ($\overline{D}$) and standard deviation (σ_d) are defined as

$$\overline{D} = \frac{\sum_i N_i D_i}{\sum_i N_i} \quad \text{and} \quad \sigma_d = \left[\frac{\sum_i N_i (D_i - \overline{D})^2}{\sum_i N_i}\right]^{1/2},$$

respectively, where N_i is number concentration of droplets with diameter D_i. Skewness (Sk) and kurtosis (Ku) are defined as

$$\text{Sk} = \frac{\sum_i N_i (D_i - \overline{D})^3}{\sigma_d^3 \sum_i N_i} \quad \text{and} \quad \text{Ku} = \frac{\sum_i N_i (D_i - \overline{D})^4}{\sigma_d^4 \sum_i N_i},$$

respectively. The time variations of the statistical parameters of droplet spectrum for simulation in Fig. 2 are shown in Fig. 4. Figure 4 also shows $\overline{D}$ and σ_d. Below cloud base $\overline{D}$ was nearly constant (during the first 3 min after starting simulation). Both $\overline{D}$ and σ_d sharply increased during updraft above cloud base. During the ripening process (from 0.37 to 3 h) $\overline{D}$ and σ_d continuously increased with time. The increase in σ_d is an indication of broadening in the droplet spectrum.

Dispersion (δ) is defined as $\sigma_d/\overline{D}$. The time variation of δ is shown in Fig. 4b. Due to different behavior of $\overline{D}$ and σ_d, δ changed with time. However, the changes of δ were slow and the values of δ were on the order

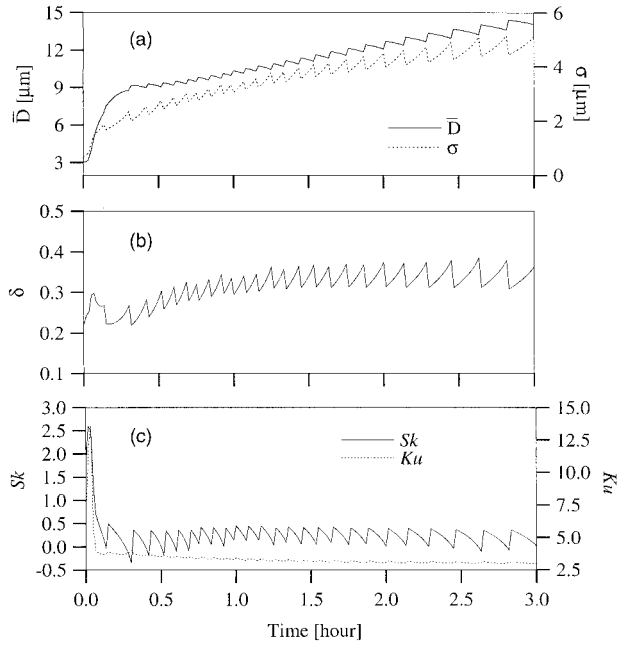

FIG. 4. Time variation of (a) $\overline{D}$ and σ; (b) δ; and (c) Sk (skewness) and Ku (kurtosis) for the simulation in Fig. 2.

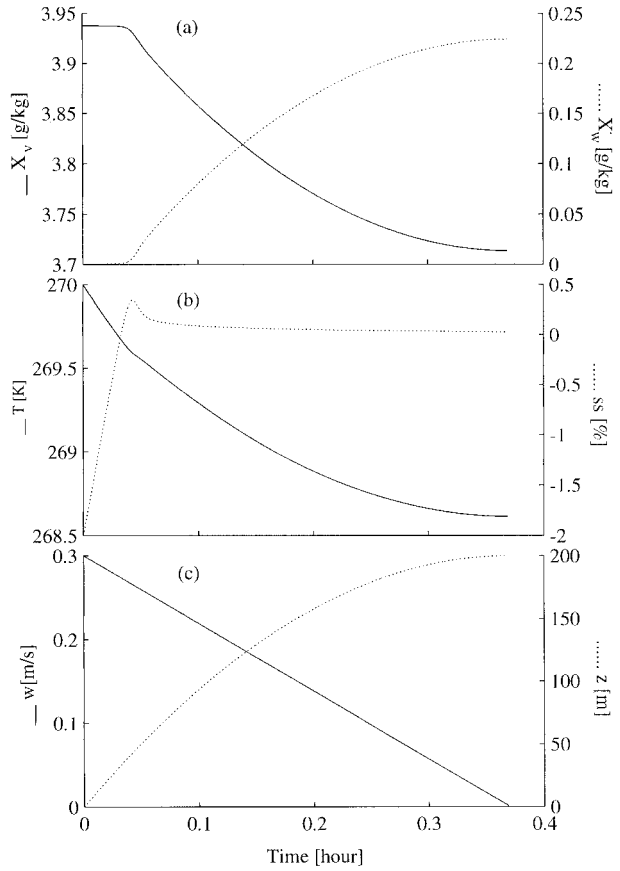

FIG. 5. Time changes of various parameters for the simulation in Fig. 2 during the vertical displacement of air parcel (from 0.0 to 0.37 h); (a) time variation of X_v and X_w, (b) T and s, and (c) w and vertical displacement (z).

of 0.3. From aircraft measurements in cumulus clouds, Warner (1969a) reported values of δ from 0.1 to 0.4.

Time variations of Sk and Ku are shown in Fig. 4c. Both parameters strongly changed in response to the changes of $\overline{D}$ and σ_d during updraft (especially before activation). After the updraft stage ($t > 0.37$ h) they became nearly constant. The positive values of Sk ($\sim$0.25) indicate that the droplet spectra are positively skewed; for example, the spectrum is not symemetric and has a longer tail at the large end and a shorter tail at the low end. The level of Ku (flatness) was about 3. Warner (1969a) reported 0.25 and 3.5 for median Sk and Ku respectively, from nearly 1000 samples of measurements in cumulus clouds.

The time changes of various parameters during the updraft stage (0 to 0.37 h) are shown in Fig. 5. No significant changes in water vapor mixing ratio (X_v) and liquid water mixing ratio (X_w) took place before s exceeded 0. The peak s occurred just above cloud base. Due to condensation on the droplets, X_v was decreasing while X_w was increasing during updraft.

From 0.37 to 3 h, the cloud was steady ($w = 0$). Because of the salinity and curvature effects of droplets the internal processes in the cloud did not stop during the steady-state stage ($w = 0$). Microphyscial parameters continued to change with time (Fig. 6). The variation of droplet number concentration is shown in Fig. 6a. The maximum number concentration was about 520 cm^{-3} (during updraft). The number concentration continuously decreased to around 120 cm^{-3} (during the ripening process). The decrease in number concentration was associated with a decrease in s. Since $w = 0$ (from 0.37 to 3 h) there was no source of s from adiabatic cooling. The only source of s was the evaporation of smaller droplets and the only sink of s was the growth of larger droplets (note that without curvature and salinity terms, the s left over from the updraft would be used up in less than 10 s without an increase on the size of droplets). The process of growth of droplets is different from the conventional condensational growth of droplets in updrafts by adiabatic cooling. Due to the imbalance between the rate of release of water vapor from the evaporation of small droplets and the rate of condensation of water vapor on the large droplets, there are small variations in X_v, X_w, s, and temperature (T) with time. These variations are shown in Figs. 6b and 6c. The small-scale steps in these parameters occurred when individual size classes evaporated.

b. *Response of the ripening process to the changes in the salinity of droplets*

Numerical simulations were performed to test the changes in the salinity of CCN particles on broadening

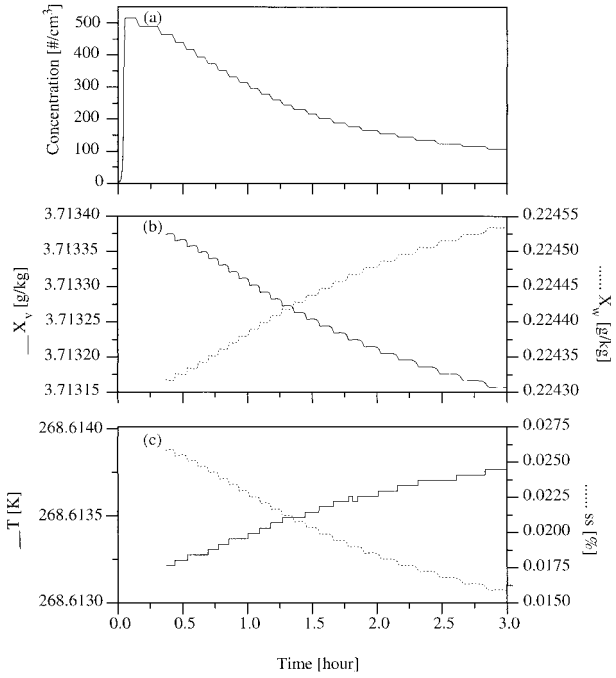

FIG. 6. Time changes of various parameters for the simulation in Fig. 2 during the evolution of cloud parcel at $z = 200$ m with $w = 0$; (a) droplet concentration with diameter >2.4 μm; (b) X_v and X_w; (c) T and s.

of droplet spectra and growth of large droplets. Eight different simulations were performed with eight different CCN spectra. The largest dry sizes of the CCN particles in the spectra were assumed to be 0.5, 0.6, 0.7, 0.8, 0.9, 1.0, 1.1, and 1.2 μm in radius for simulations 1–8, respectively. The CCN spectrum for each simulation was determined by extrapolation of measurements of Hobbs et al. (1985b) as described in section 2b. The model aerosol spectrum used in these simulations is shown in Fig. 1a. Depending on the simulation, a part of the aerosol spectrum from 0.02 μm to the defined maximum size of CCN in Fig. 1a was used and the rest of the spectrum was truncated. The cumulative distributions of CCN as a function of size and activity spectra for the simulations are shown in Figs. 7a and 7b, respectively. In each case there are 100 CCN classes. The masses of the soluble part of the largest CCN were 7.3×10^{-13}, 1.2×10^{-12}, 2.0×10^{-12}, 3.0×10^{-12}, 4.3×10^{-12}, 5.9×10^{-12}, 7.8×10^{-12}, and 1.0×10^{-11} g for simulations 1–8, respectively. The vertical velocity for these simulations is given in Eq. (2). The other initial conditions are the same as described in section 2b.

The results are shown in Fig. 8. Figures 8a–h corresponds to simulations 1–8, respectively. It is shown that there is broadening of the droplet spectra for all simulations. The broadening toward larger sizes increases with increasing salinity and takes place both during updraft (0–0.37 h) as well as during steady-state stages ($w = 0$) from 0.37 to 3 h. Although the sizes of the

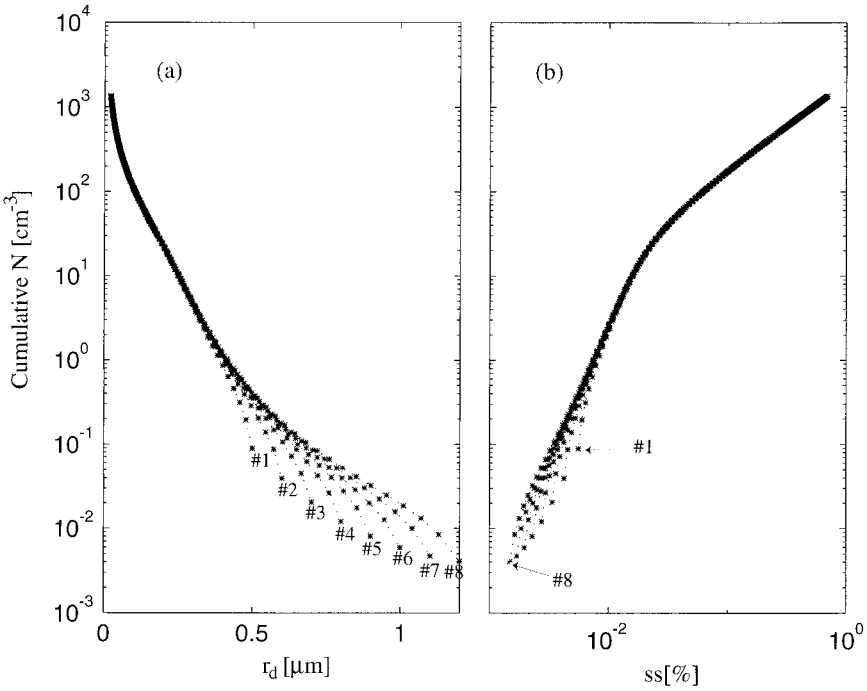

FIG. 7. (a) Cumulative distributions of CCN particles and (b) activity spectra. The numbers 1–8 correspond to simulations 1–8, respectively.

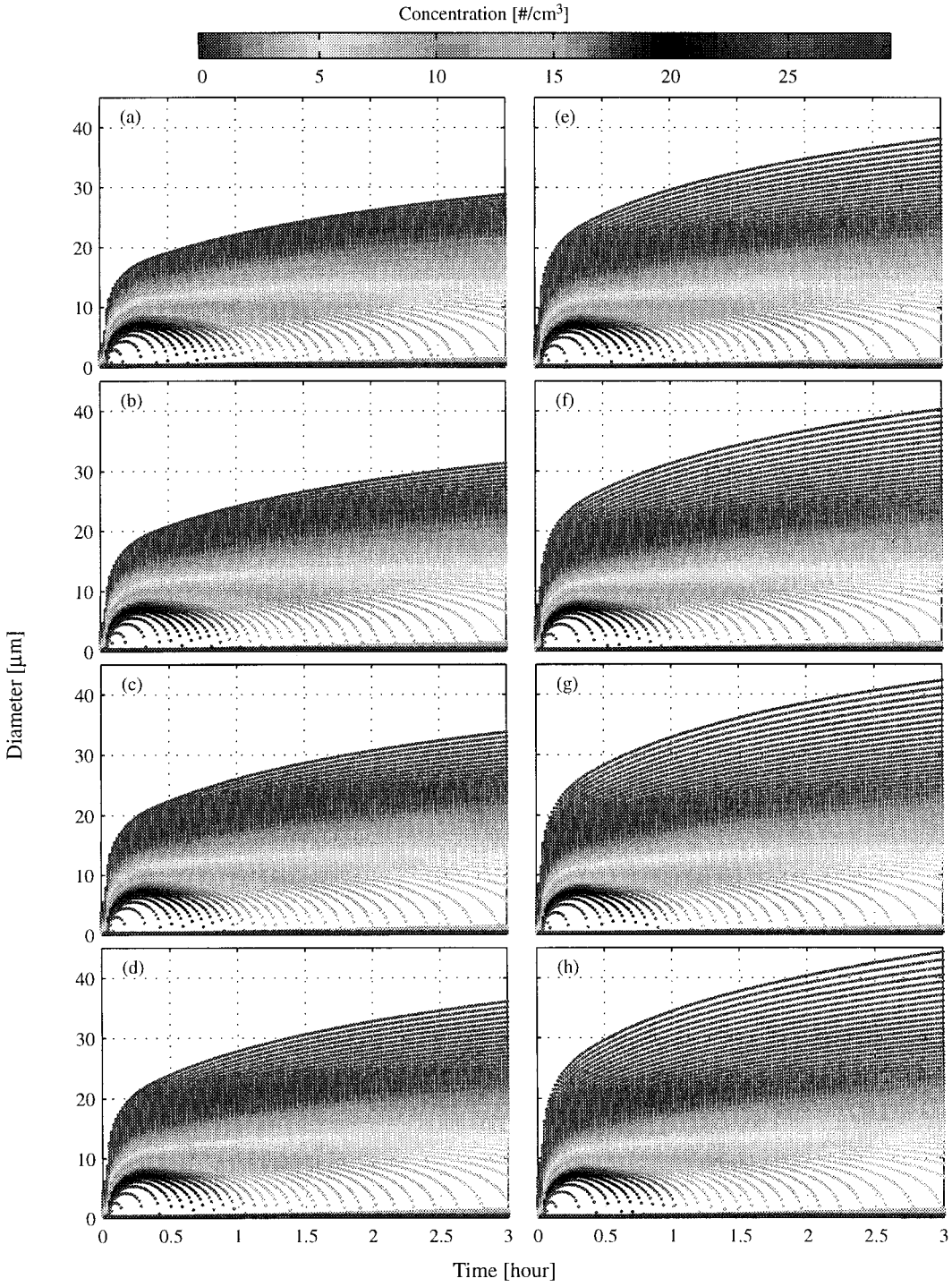

FIG. 8. Evolution of droplet size spectra for the salinity simulations. The largest dry size of CCN is (a) 0.5, (b) 0.6, (c) 0.7, (d) 0.8, (e) 0.9, (f) 1.0, (g) 1.1, and (h) 1.2 μm in radius. The concentration bar at the top of the figure is related to the concentrations of droplets and particles in each class.

large droplets get bigger, the number concentrations get smaller (similar to Fig. 6a). The largest droplet diameters were about 18 and 28 μm at 0.37 h in simulations 1 (Fig. 8a) and 8 (Fig. 8h), respectively. Therefore, increases in salinity in the CCN spectrum result in increases in the growth rates of large droplets during the updraft stage.

From 0.37 to 3 h the parcel was steady ($w = 0$).

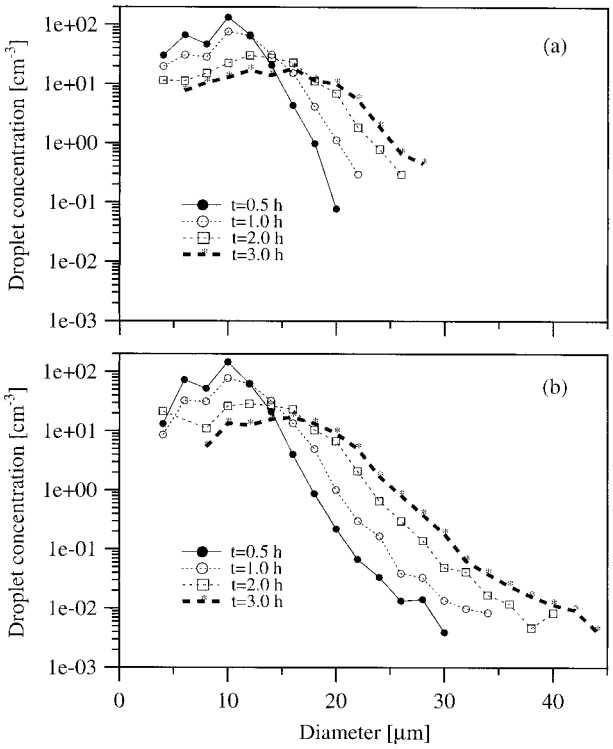

FIG. 9. Droplet spectra at 0.5, 1.0, 2.0, and 3 h for (a) simulation with the largest CCN of 0.5 μm in radius (Fig. 8a) and (b) simulation with the largest CCN of 1.2 μm in radius (Fig. 8h).

During this time interval, the largest droplet diameters increased to 29 and 45 μm in simulations 1 (Fig. 8a) and 8 (Fig. 8h), respectively. During the steady-state stage, the increases in the largest droplet diameters were around 11 μm for simulation 1 and 17 μm for simulation 8. The corresponding dry radii of the largest CCN were 0.5 and 1.2 μm for simulations 1 and 8, respectively. Therefore, an increase in the salinity of CCN spectrum results in acceleration of broadening of droplet spectrum and growth of large droplets during the ripening process.

The other parameters (X_v, X_w, s, T, and cloud droplet concentration) changed similarly to the changes shown in Fig. 6.

Figure 9 shows the droplet spectra (concentration as a function of size) at 0.5, 1, 2, and 3 h for the simulations in Fig. 8. Figures 9a and 9b correspond to simulations 1 and 8, respectively. It is seen that spectral broadening toward large sizes increases with increasing salinity of CCN.

c. Roles of vertical turbulent fluctuations on the ripening process in an adiabatic closed cloud parcel

The ripening process does not require turbulent fluctuations of s. For example, during a turbulent updraft some droplets will grow while some others may evaporate in a cloud. Similarly, during a turbulent downdraft some droplets will evaporate while some others may grow. All the activated cloud droplets may grow (evaporate) during updraft (downdraft). The rates of growth/evaporation of droplets will be different due to differences in s^*. In the presence of turbulent fluctuations, the ripening process shows up at times longer than the characteristic times of turbulent fluctuations as a superimposed independent process in the system. In this section, numerical simulations were performed to show this phenomena.

Numerical simulations were performed for the cloud droplet spectra evaluations in cloud parcels with steady state, sinusoidal oscillations, and turbulent fluctuations after the initial updraft. Initial conditions are the same for the three cases as described in section 2b. The largest dry CCN radius was assumed to be 1 μm for all cases.

The vertical velocity profile during the updraft stage was the same for all simulations and is given as

$$w(t) = [w_o - (w_o^2/2H)t] \qquad 0 \le t < t_H, \tag{4}$$

where $w_o = 0.3$ m s^{-1}, $H = 200$ m, and $t_H = 2H/w_o$ (0.37 h). Thus, the updraft stage is 0.37 h [note that $\int_0^{t_H} w\,dt = H$ and $w(t_H) = 0$]. The vertical velocity profiles from 0.37 to 3 h for steady state, sinusoidal oscillations, and turbulent fluctuations are given as

$$w(t) = \begin{cases} 0 & \text{Steady} \\ w_s \sin\left[\dfrac{2\pi}{\tau}(t - t_H)\right] & \text{Sinusoidal} \\ \text{Turbulent} & \text{Turbulent,} \end{cases} \tag{5}$$

where $w_s = 0.5$ m s^{-1} and $\tau = \pi\Delta z/w_s$ is the period of oscillations. The amplitude of the oscillations (Δz) was assumed to be 80 m. Thus, the period of the oscillations was 503 s. Turbulent fluctuations of w were generated from uniformly distributed random fluctuations. The random fluctuations are constrained to fit the energy–wavenumber relation $E(k) = \alpha\varepsilon^{2/3}k^{-5/3}$ in the inertial subrange (Tennekes and Lumley 1990), where E is the energy at wavenumber k, ε is the eddy dissipation rate, and α is a constant (1.5). The value of ε was assumed to be 10^{-4} m^2 s^{-3} (consistent with the turbulent level in stratiform clouds). Thus, the generated turbulent fluctuations were not totally random fluctuations (white noise) and they have the energy–wavenumber relation as observed in a turbulent flow in the atmosphere. The vertical scales of the turbulent fluctuations were further constrained to be on the order of 50 m.

The results are shown in Fig. 10. Figures 10a, 10b, and 10c show the evolution of droplet spectra in cloud parcels at steady state, undergoing sinusoidal oscillations, and undergoing turbulent fluctuations, respectively. Droplet spectra broadening are common in all cases. The numerical simulation for the steady-state case (Fig. 10a) is identical to the numerical simulations in Fig. 2 and 8f. The response of droplets to sinusoidal oscillations and turbulent fluctuations masks the rip-

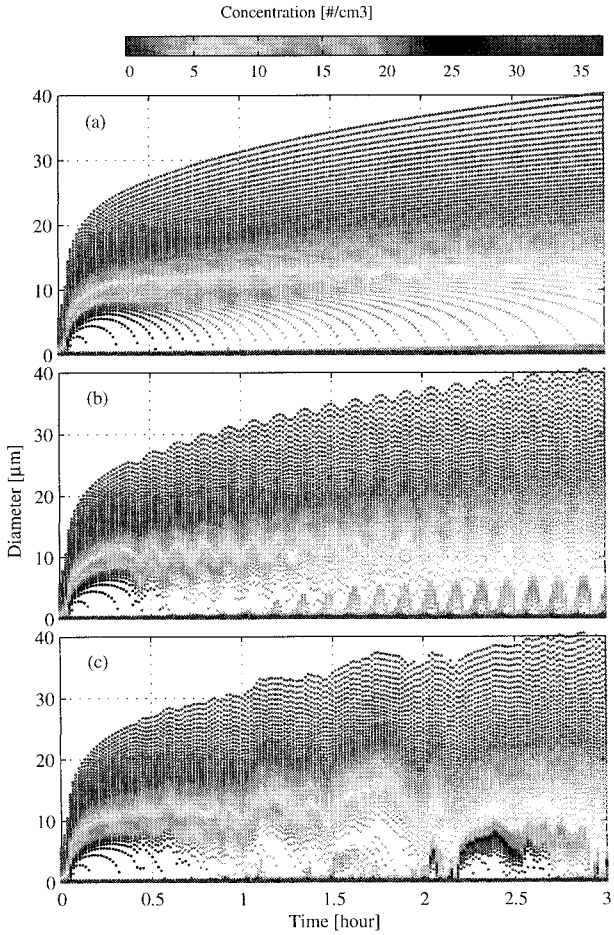

FIG. 10. Evolution of droplet spectra in cloud parcels at (a) steady state, (b) sinusoidal oscillations, and (c) turbulent fluctuations. All the initial conditions were the same for all cases. The concentration bar at the top of the figure is related to the concentrations of droplets and particles in each class.

ening process at timescales smaller than the timescales of oscillations or turbulent fluctuations (Figs. 10b,c). However, the ripening process showed up as an independent process at timescales longer than the timescale of oscillations and turbulent fluctuations. The ripening process is the main reason for the broadening in all cases. Growths of the largest droplets in cloud parcels at steady state, undergoing sinusoidal oscillations or turbulent fluctuations were comparable to each other. For a closed cloud parcel, the main difference between evolution of droplet spectrum in a steady-state parcel and the evolution of droplet spectra in cloud parcels undergoing sinusoidal or turbulent fluctuations is the activation of fresh CCN or haze particles in cloud parcels undergoing sinusoidal oscillations or turbulent fluctuations. The activation of haze or fresh CCN during updrafts (wave oscillations or turbulent fluctuations) results in generation of secondary newly formed modes at small sizes relative to the primary modes at large sizes; therefore, the droplet spectra become bimodal.

4. Discussion

Aerosol and CCN spectra are important factors for the ripening process. The ripening process depends on the salinity and curvature of the droplets. The strong curvature effect of small droplets results in faster growth of large droplets. An increase in the salinity (size of CCN) increases the broadening of droplet spectra and the growth of large droplets. The existence of CCN with diameter >1 μm is important for the growth of large droplets by the ripening process. Aerosols with diameters on the order of 5 μm with low concentrations are commonly observed over continental regions (Willeke and Whitby 1975; Hobbs et al. 1985a; among others). The existence of aerosols with diameters up to 5 μm have been observed over oceans by Junge (1972), Meszaros and Vissy (1974), Jensen et al. (1996), among others. Chemical composition analysis of aerosols shows the existence of water soluble [NaCl, $(NH_4)_2SO_4$, and others], water insoluble (such as silicates), and organic components with water soluble and water insoluble materials. A chemical analysis of aerosols over the rural continental regions of West Germany showed that aerosols with diameters from 0.2 to 0.6 μm were about 80% water soluble, aerosols with diameters from 0.6 to 2 μm were about 70% water soluble, and aerosols with diameter >2 μm were about 50% water soluble materials (Warneck 1988). Junge (1954) reported that aerosols over the Atlantic coast with diameters from 0.16 to 1.6 μm are almost entirely sulfate and ammonia while aerosols with diameter from 1.6 to 16 μm contain variable materials and sometimes contain considerable amounts of nitrate and sodium chloride.

Physical processes in the cloud parcel do not stop after initial updraft. Because of salinity and curvature effects, droplet spectrum and droplet number concentration continuously change with time. The estimated number concentration of droplets from the analytical derived relations (Squires 1958; Twomey 1959) are only valid for a short time in the updraft stage of cloud. The number concentration decreases continuously with time (Fig. 6a). The results in this study were obtained by assuming that the parcel was steady state ($w = 0$) after the initial updraft. The existence of turbulent fluctuations will also tend to fluctuate droplet number concentrations.

The cloud model used herein was a simple, adiabatic, closed parcel model. Due to turbulent mixing, entrainment, gravitational settlement of droplets, radiative heating or cooling, collision/coalescence instability, precipitation, and other microphysical processes, the processes in real clouds will deviate from the processes in this idealized cloud model. These simplifications were not necessary for the ripening process and the ripening process will exist in any kind of cloud in any environment as long as there exist droplets with different salinity and size. The relative importance of the ripening process on the formation of droplet spectra will be dif-

ferent for different clouds. For instance, in a cumuliform cloud, mixing and entrainment processes are probably more important than the ripening process.

The existence of other processes, such as mixing, entrainment, gravitational settlement of droplets, and collision–coalescence instability may increase or decrease the importance of the ripening process. For example, a turbulent mixing process that brings small and large droplets together may accelerate the ripening process and, thus, growth of large droplets. Thus, an extension of this model into a more realistic cloud model (e.g., including turbulent mixing between cloud parcels) may produce more realistic results in more realistic timescales.

Comparison with previous studies

In the present simulations, the basic cloud physics equations are the same as in many previous numerical simulations by other authors. Previous numerical studies failed to recognize the droplet spectra broadening and formation of large droplets by the ripening processes. The reasons are as follows. 1) There were few CCN classes in the models. 2) The evolution of droplet spectra was simulated during only updrafts. The ripening process may appear in slow updraft cases if the number of classes of CCN is large. The reason is that the slow updrafts do not provide sufficient s for the growth of all the activated droplets after the peak s; thus, droplets with high s^* will evaporate during updraft. Srivastava (1991) noted the evaporation of smaller droplets during a slow updraft but he did not recognize that the process of ripening was occurring because the ripening process was superimposed on the condensation process during updraft. 3) In the previous numerical studies an air parcel containing a few classes of CCN was displaced a few kilometers vertically; thus, the size of the smallest droplets in the parcel was on the order of 10 μm. Therefore, the effect of curvature was not sufficient to evaporate the droplets during updraft. 4) The ripening process was not isolated from condensation by setting $w = 0$ after the initial updraft. Hagen (1979) conducted numerical simulations for the support of cloud chamber studies and noted the droplet spectrum broadening by evaporation of small droplets. Although, he referred to the ripening process as Ostwald ripening and he suggested that Ostwald ripening may be a possible mechanism for droplet spectra broadening in the atmosphere, the cloud physics community apperently did not recognize its importance.

Korolev (1995) argued that a droplet size spectrum is irreversible for cycling growth and evaporation. Based on numerical studies he concluded that turbulent fluctuations of *s* result in droplet spectra broadening and formation of large droplets. A droplet spectrum containing droplets with different salinity and size is an unstable system (changes with time are irreversible) itself. An external forcing mechanism is not necessary for the irreversibility of the system. Thus, Korolev's (1995) argument on the irreversibility of droplet spectrum for cycling growth and evaporation is not valid. Numerical simulations (Fig. 10) showed that droplet spectra broadening in closed cloud parcels at steady state, and undergoing sinusoidal oscillations or turbulent fluctuations, are similar to each other in general (except responses of droplet spectra to vertical up and down motions at timescales on the order of period oscillations or characteristic time of turbulent fluctuations). Droplet spectra broadening and growth of the largest droplets in three cases were comparable to each other. Therefore, the turbulent fluctuations of *s* were not responsible for the droplet spectra broadening and formation of large droplets. Thus, the conclusion of Korolev (1995) that the turbulent fluctuations of *s* result in droplet spectra broadening and formation of large droplets is not valid.

Hudson and Svensson (1995) observed that cloud droplet concentration was inversely related to the mean diameter ($\overline{D}$). This inverse relation indicates that in regions of high droplet concentration the $\overline{D}$ was low and in the low droplet concentrations $\overline{D}$ was high. Hudson and Yum (1997) showed positive correlation between σ_d and $\overline{D}$ from measurements in marine stratus clouds. This positive correlation indicates that the regions of large $\overline{D}$ correspond to broad droplet size spectra and the regions of small $\overline{D}$ correspond to narrow droplet size spectra. Similarly, the numerical simulations in this paper showed that droplet concentration decreases while the $\overline{D}$ and σ_d increase with time. Thus, high droplet concentrations correspond to low $\overline{D}$ and low droplet concentrations correspond to high $\overline{D}$. Therefore, numerical simulations indicate an inverse relation between droplet concentration and $\overline{D}$. Both $\overline{D}$ and σ_d were increasing with time, which is an indication that $\overline{D}$ and σ_d are positively correlated. Thus, the model predictions are consistent with observations. However, because of the variety of different physical processes in clouds (e.g., mixing processes between cloud and clear air and between different cloud parcels, and turbulence) the positive corelation between $\overline{D}$ and σ_d may not be the case all the time. Other important points to note are that the numerical simulations in this paper were from a Lagrangian cloud parcel model, that it would be hard to relate directly to the observations, and that the simulations were up to 3 h, which is longer than most of the microphysical processes in clouds.

5. Conclusions

The ripening process in clouds occurs due to thermodynamic instability of droplet spectra. This instability in the droplet spectra is only due to the existence of droplets with different salinity and size in the droplet spectra. It was shown that supersaturation was maintained during the ripening process. The ripening process is independent of turbulent fluctuations of supersaturation at a given level in a closed cloud parcel. Turbulent

fluctuations of vertical velocity or wave oscillations result in the formation of bimodal droplet spectra as suggested by other authors. Due to the ripening process, droplet number concentration decreases while mean droplet size increases with time after initial updraft (peak supersaturation) in the absence of vertical turbulent fluctuations.

The ripening process is dependent on the CCN spectra, height from cloud base, temperature, condensation coefficient, and vertical velocity profile during updraft. The relative roles of these parameters will be discussed in future parts of this series.

Acknowledgments. This research was initiated and developed by Fikrettin Çelik during Ph.D. studies at the University of Wyoming. This research was funded by NSF Grant ATM-9523434.

APPENDIX

Cloud Model

A Lagrangian cloud model is used for simulation of cloud droplet spectrum evolution. The evolution of droplet spectra is simulated considering only the condensation process. Mixing, gravitational fall speed, collision and coalescence growth, and ice phase processes are excluded. This is a closed, reversible adiabatic parcel model. The evolution of droplet spectra is simulated using the following equations.

a. Pressure equation

Starting from the vertical component of the equation of motion and using the ideal gas equation for an air parcel containing dry air (m_d) and water vapor (m_v) the equation for the pressure can be derived as

$$\frac{dp}{dt} = -\frac{p}{R_m T}\left(G + \frac{dw}{dt}\right)w, \tag{A1}$$

where p is pressure; T is temperature; ρ is the density of air; $R_m = (m_d R_d + m_v R_v)/(m_d + m_v)$ is the gas constant for moist air; R_d and R_v are the gas constants for dry air and water vapor, respectively; G is the acceleration due to gravity; and w is the vertical velocity. In this derivation the motion is assumed to be frictionless; earth rotation and curvature terms are neglected.

b. Temperature equation

The entropy equation for a system containing a unit mass of dry air is given as

$$dS = (c_{pd} + X_v c_{pv} + X_w c_w)d\ln T - (1 + X_v)R_m d\ln p + l_v dX_v/T,$$

where X_v and X_w are the mixing ratios of water vapor and liquid water, respectively; $T_o = 273.15$ K; c_{pd} and c_{pv} are the specific heats for dry air and water vapor at constant pressure, respectively; c_w is the specific heat of liquid water; and l_v is the specific latent heat of condensation and changes with T (Rogers and Yau 1989) written as

$$l_v(T) = 2.503 \times 10^6 - (c_w - c_{pv})(T - T_o) \quad [\text{J kg}^{-1}].$$

An adiabatic and reversible system is an isentropic system (entropy of the system is conserved). Taking the time derivative of the entropy equation, setting $dS/dt = 0$, substituting for dp/dt from Eq. (A1), and solving for dT/dt gives the temperature equation

$$\frac{dT}{dt} = \frac{1}{c_{pm}}\left[-l_v\frac{dX_v}{dt} - (1 + X_v)\left(G + \frac{dw}{dt}\right)w\right], \tag{A2}$$

where $c_{pm} = c_{pd} + X_v c_{pv} + X_w c_w$.

c. Equation for condensational growth/evaporation

$$\frac{dr}{dt} = (s - s^*)\Psi/r, \tag{A3}$$

where

$$\Psi = \left[\frac{l_v\rho_l}{KTf_1(\alpha)}\left(\frac{l_v}{R_v T} - 1\right) + \frac{\rho_l R_v T}{De_s f_2(\beta)}\right]^{-1};$$

r is the cloud droplet radius; s is the ambient supersaturation; s^* is the equilibrium supersaturation; ρ_l is the density of liquid water; K and D are the thermal conductivity and molecular diffusion coefficients of air, respectively; the functions $f_1(\alpha)$ and $f_2(\beta)$ are the kinetic correction functions for heat and mass diffusion, respectively; and e_s is the saturation vapor pressure. For information on the derivation of Eq. (A3) see Rogers and Yau (1989) or any other textbook on cloud physics. Here K and D change with T and p (Pruppacher and Klett 1978) as

$$K(T) = 2.3823 \times 10^{-2} + 7.1176 \times 10^{-5}(T - T_o) \quad [\text{J m}^{-1}\,\text{s}^{-1}\,\text{K}^{-1}],$$

$$D(T, p) = 2.11 \times 10^{-5}(T/T_o)^{1.94}(p_o/p) \quad [\text{m}^2\ \text{s}^{-1}].$$

The equation for the equilibrium supersaturation (s^*) is

$$s^* = \exp\left(\frac{2\sigma}{\rho_l R_v T r}\right)\left(1 + \frac{i\varepsilon M_w \rho_d r_d^3}{M_s(\rho' r^3 - \rho_d r_d^3)}\right)^{-1} - 1,$$

where σ is the surface tension; and changes with T and M (molarity) (Pruppacher and Klett 1978) are

$$\sigma(T, M) = 7.61 \times 10^{-2} - 1.55 \times 10^{-4}(T - T_o) + 2.17 \times 10^{-3}M \quad [\text{J m}^{-1}],$$

where i is the van't Hoff factor; M_w and M_s are the molecular weight of water and dissolved substances; ρ' is the mean density of the solution; ε is the mass fraction of salt in the dry aerosol; r_d and ρ_d are the radius and

density of CCN particles, respectively; $T_o = 273.15$ K; and $p_o = 101\,325$ Pa. The exponential part of the above equation is the curvature term. Note that ρ_l in the s^* equation is density of pure water and curvature dependence of activity coefficient of water in a solution was suggested to be negligible (Pruppacher and Klett 1978). For more information on the equilibrium supersaturation equation see Fletcher (1962), Pruppacher and Klett (1978), and Warneck (1988).

The kinetic correction functions in Eq. (A3) are defined by Fukuta and Walter (1970) as

$$f_1(\alpha) = \frac{r}{r + \dfrac{K\sqrt{2\pi R_m T}}{\alpha p(c_v + R_m/2)}} \quad \text{and} \quad f_2(\beta) = \frac{r}{r + \dfrac{D}{\beta}\sqrt{\dfrac{2\pi}{R_v T}}},$$

where α is the thermal accommodation coefficient and β is the condensation coefficient.

The derivation of the growth equation [(A3)] contains assumptions. Some of the main assumptions are listed here. 1) The droplet is assumed to be spherical and the water vapor around the droplet is isotropically distributed. With this assumption the inhomogenity in the distribution of water vapor around the droplet is neglected. 2) Droplet growth or evaporation is represented by the gradient of water molecules and there is no source and sink of water molecules except the droplet surface and surrounding air. 3) It is assumed that the release of latent heat at the droplet surface is conducted away from the droplet as fast as it is released. Thus the droplet surface temperature (T_r) is assumed to be steady state (Note that this assumption does not mean that T_r is assumed to be the air temperature (around the droplet). 4) Droplet growth is assumed to be quasi-static. For small s this is a good assumption. For large positive or negative s this assumption results in error (e.g., a droplet falling from cloud base throughout the subsaturated environment). During the formation of cloud, peak s occurs ($\sim$0.2% for stratiform cloud) for a very short time; thereafter, s drops to very low values ($\sim$0.02%). This assumption is a valid assumption for the physical processes studied in this paper. 5) Vapor density at the droplet surface is equal to the saturation vapor density at the droplet temperature. Due to the above assumptions the error in the growth equation may be a few percent (Young 1993).

During the activation of CCN the solution in the particles is not significantly dilute; therefore, the solution is not an ideal solution and Henry's and Raoult's laws are not valid. The ideal solution assumption in the derivation of s^* results in error in the calculations. Low (1969) and Young and Warren (1992) introduced composition-dependent van't Hoff factor (i) for nonideal solutions. Recently, Konopka (1996) reexamined the derivation of s^* and argued that for nonideal solutions critical supersaturation (S_c) increases up to 25% if compared with the ideal approximation. The Konopka (1996) comparison was for an H_2SO_4–H_2O system and it was shown that the increase in critical supersaturation (S_c) was for a small amount of H_2SO_4 in the droplet ($\sim 10^{-20}$ kg). Activation of droplets at that salinity requires high supersaturations during the formation of cloud ($\sim$4%), which is well above the peak supersaturation ($<$0.5%) found in stratiform clouds.

Nonideality of droplets is important during the formation of cloud (activation of CCN). After the updraft stage, the size of droplets will be significantly large so that the solution in the droplets is dilute. Thus, the ideal solution assumption is valid. Nonideality in the evaporating small droplets increases due to increase in the molality of salt by decreasing size of droplets.

An overall increase/decrease in s^* for all the CCN particles due to nonideality of solution of droplets in all sizes will not change the droplet concentration during the formation of cloud, because supersaturation during updrafts will be higher/lower to activate droplets to maintain adiabatic liquid water content. Changes of s^* at different sizes would be critical during the formation and evolution of cloud. Because the growth of droplets is determined by the relative difference between s and s^* during updraft, and the ripening process during the evolution of cloud occurs due to the relative differences of s^* among droplets.

d. Supersaturation (ss) equation

Starting from the definition of saturation ratio and using the pressure equation [(A1)], temperature equation [(A2)], Clausius–Clapeyron equation, and by approximating $e \cong pX_v/\varepsilon$, the equation of s can be written as

$$\frac{ds}{dt} = (s+1)\left[\frac{(X_v+1)l_v}{c_{pm}R_v T^2} - \frac{1}{R_d T}\right]\left(G + \frac{dw}{dt}\right)w - \left[\frac{p}{\varepsilon e_s(T)} + \frac{(s+1)l_v^2}{c_{pm}R_v T^2}\right]\frac{dX_w}{dt}, \tag{A4}$$

where $\varepsilon = 0.622$.

e. Equation for conservation of water (liquid + vapor)

Let us consider a system containing dry air, water vapor, and liquid water with masses of m_d, m_v, and m_w, respectively. In the system, the total amount of water ($m_t = m_v + m_w$) and the amount of dry air are conserved. The transformation from water vapor to liquid water or liquid water to water vapor causes the amount of liquid water and water vapor to change with time. Thus, the equation for the conservation of water can be written as

$$\frac{dX_v}{dt} + \frac{dX_w}{dt} = 0. \tag{A5}$$

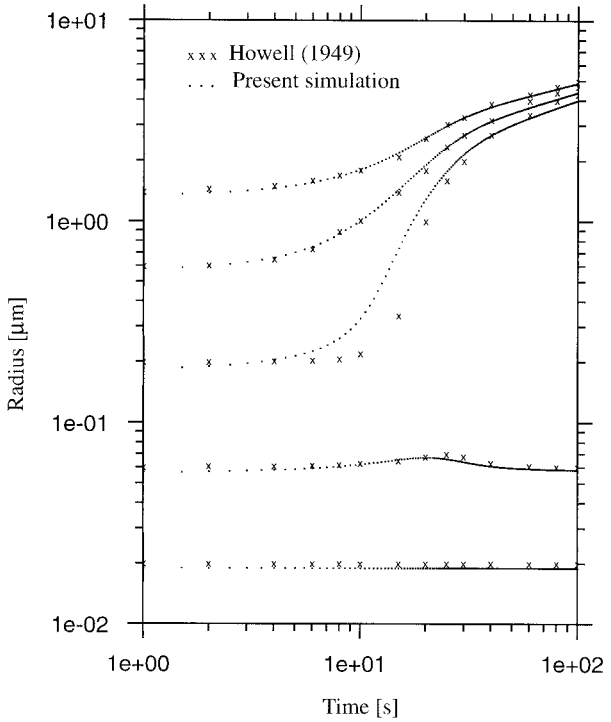

FIG. A1. Comparison of present model simulation with Howell's (1949) simulation.

f. Equation for liquid water mixing ratio

The amount of liquid water in an air parcel is determined by integrating the liquid water over all the droplet sizes

$$m_w = \frac{4\pi}{3}\rho' \int N(r) r^3 \, dr - \frac{4\pi}{3}\rho_d \int N(r_d) r_d^3 \, dr_d,$$

where $N(r)$ and $N(r_d)$ are the number concentration of droplets with radius r and number concentration of CCN with radius r_d; here ρ' is the density of the solution. The first integral on the right-hand side is the total amount of mass in the parcel and the second integral is the total mass of the aerosol in the parcel. Dividing the above equation by the mass of dry air (m_d), taking the time derivative of the resulting equation, by approximating $\rho' \cong \rho_l = \text{const.}$, and setting $dN(r)/dt = 0$ (the parcel is a closed system), the time derivative of the liquid water mixing ratio (X_v) becomes

$$\frac{dX_w}{dt} = \frac{4\pi\rho_l}{m_d} \int N(r) r^2 \frac{dr}{dt} \, dr. \qquad \text{(A6)}$$

In the continental regions $(NH_4)_2\,SO_4$ is the major constituent of aerosols (Junge 1954; Junge and Werby 1958; Warneck 1988). Thus, $(NH_4)_2\,SO_4$ is assumed for the dissolved material in the droplets for continental clouds. Equilibrium sizes of the CCN particles at the initial relative humidity (98%) are calculated before starting numerical simulation.

Equations (A1)–(A6) are solved using the Runge–Kutta fourth-order numerical method with time step of 0.005 s. The Runge–Kutta fourth-order method is a strongly stable method with local truncation error $O(\Delta t^4)$. For more information on the Runge–Kutta methods see Burden and Faires (1985).

Integration time was assumed to be 3 h because stratiform clouds have timescales on this order.

A direct comparison has been performed with the classical simulation of Howell (1949) and presented in Fig. A1. These results indicate that no gross errors were present in the software.

REFERENCES

Baker, M. B., and J. Latham, 1979: The evolution of droplet spectra and the rate of production of embryonic raindrops in small cumulus clouds. *J. Atmos. Sci.,* **36,** 1612–1615.

——, R. G. Corbin, and J. Latham, 1980: The influence of entrainment on the evolution of cloud droplet spectra. I: A model of inhomogeneous mixing. *Quart. J. Roy. Meteor. Soc.,* **106,** 581–598.

Beard, K. V., and T. H. Ochs, 1993: Warm-rain initiation: An overview of microphysical mechanisms. *J. Appl. Meteor.,* **32,** 608–625.

Burden, R. L., and J. D. Faires, 1985: *Numerical Analysis.* 3d ed. Prindle, Weber, and Schmidt, 676 pp.

Cooper, W. A., 1989: Effects of variable droplet growth histories on droplet size distributions. Part I: Theory. *J. Atmos. Sci.,* **46,** 1301–1311.

Cotton, W. R., and R. A. Anthes, 1989: *Storm and Cloud Dynamics.* Academic Press, 883 pp.

Everett, D. H., 1988: *Basic Principles of Colloid Science.* Royal Society of Chemistry, 243 pp.

Fletcher, N. H., 1962: *The Physics of Rainclouds.* Cambridge University Press, 386 pp.

Frisbie, R. P., and J. G. Hudson, 1993: Urban cloud condensation nuclei spectral flux. *J. Appl. Meteor.,* **32,** 666–676.

Fukuta, N., and L. A. Walter, 1970: Kinetics of hydrometeor growth from a vapor-spherical model. *J. Atmos. Sci.,* **27,** 1160–1172.

Hagen, D. E., 1979: A numerical cloud model for the support of laboratory experimentation. *J. Appl. Meteor.,* **18,** 1035–1043.

Harding, D. D., 1977: *Microphysical Response of Cloud Droplets in Fluctuating Updraft.* Ph.D. dissertation, University of Michigan, 167 pp.

Hobbs, P. V., D. A. Bowdle, and L. F. Radke, 1985a: Particles in the lower troposphere over the High Plains of the United States. Part I: Size distributions, elemental composition, and morphologies. *J. Climate Appl. Meteor.,* **24,** 1344–1356.

——, ——, and ——, 1985b: Particles in the lower troposphere over the High Plains of the United States. Part II: Cloud condensation nuclei. *J. Climate Appl. Meteor.,* **24,** 1358–1369.

Howell, W. E., 1949: The growth of cloud drops in uniformly cooled air. *J. Meteor.,* **6,** 134–149.

Hudson, J. G., and G. Svensson, 1995: Cloud microphysical relationships in California marine stratus. *J. Appl. Meteor.,* **34,** 2655–2666.

——, and S. S. Yum, 1997: Droplet spectral broadening in marine stratus. *J. Atmos. Sci.,* **54,** 2642–2654.

Jensen, T. L., S. M. Kreidenweis, Y. Kim, H. Sievering, and A. Pszenny, 1996: Aerosol distribution in the north Atlantic marine boundary layer during Atlantic Stratocumulus Transition Experiment/Marine Aerosol and Gas Exchange. *J. Geophys. Res.,* **101,** 4455–4467.

Johnson, D. B., 1976: Ultragiant urban aerosol particles. *Science,* **194,** 941–942.

Jonas, P. R., and B. J. Mason, 1982: Entrainment and the droplet spectrum in small cumulus clouds. *Quart. J. Roy. Meteor. Soc.,* **108,** 857–869.

Junge, C. E., 1954: The chemical composition of atmospheric aerosols, I: Measurements at Round Hill fields station, June–July 1953. *J. Meteor.,* **11,** 323–338.
——, 1972: Our knowledge of the physico-chemistry of aerosols in the undisturbed marine environment. *J. Geophys. Res.,* **77,** 5183–5200.
——, and R. T. Werby, 1958: The concentration of chloride, sodium, potassium, calcium, and sulfate in rain water over the United States. *J. Meteor.,* **15,** 417–425.
Klett, J. D., and M. H. Davis, 1973: Theoretical collision efficiencies of cloud droplets at small Reynolds numbers. *J. Atmos. Sci.,* **30,** 107–117.
Konopka, P., 1996: A reexamination of the derivation of the equilibrium supersaturation curve for soluble particles. *J. Atmos. Sci.,* **53,** 3157–3163.
Kornfeld, P., 1970: Numerical simulation for condensation of atmospheric vapor on soluble and insoluble nuclei. *J. Atmos. Sci.,* **27,** 256–264.
Korolev, A. V., 1995: The influence of supersaturation fluctuations on the droplet size formation. *J. Atmos. Sci.,* **52,** 3620–3634.
Levin, L. M., and Y. S. Sedunov, 1968: The theoretical model of the drop spectrum formation process in clouds. *Pure Appl. Geophys.,* **69,** 320–355.
Low, R. D. H., 1969: A generalized equation for the solution effect in droplet growth. *J. Atmos. Sci.,* **26,** 608–611.
Mason, B. J., and D. K. Ghosh, 1957: The formation of large droplets in small cumulus. *Quart. J. Roy. Meteor. Soc.,* **83,** 501–507.
——, and P. R. Jonas, 1974: The evolution of droplet spectra and large droplets by condensation in cumulus clouds. *Quart. J. Roy. Meteor. Soc.,* **100,** 23–38.
Meszaros, A., and K. Vissy, 1974: Concentration, size distribution and chemical nature of atmospheric aerosol particles in remote ocean areas. *Aerosol Sci.,* **5,** 101–109.
Mordy, W. A., 1959: Computations of the growth by condensation of a population of cloud droplets. *Tellus,* **11,** 16–44.
Neiburger, M., and C. W. Chien, 1960: Computations of the growth of cloud droplets by condensation using an electronic digital computer. *Physics of Precipitation, Geophys. Monogr.,* No. 5, Amer. Geophys. Union, 191–209.
Paluch, I. R., 1971: A model for cloud droplet growth by condensation in an inhomogeneous medium. *J. Atmos. Sci.,* **28,** 629–639.
Pruppacher, H. R., and J. D. Klett, 1978: *Microphysics of Clouds and Precipitation.* D. Reidel, 714 pp.
Rogers, R. R., and M. K. Yau, 1989: *A Short Course in Cloud Physics.* Pergamon, 293 pp.
Sedunov, Y. S., 1965: Fine cloud structure and its role in the formation of the cloud particle spectrum. *Izv. Atmos. Oceanogr. Phys.,* **1,** 722–731.
Squires, P., 1952: The growth of cloud drops by condensation. II. The formation of large cloud drops. *Aust. J. Sci. Res.,* **5A,** 473–499.
——, 1958: Microstructure and colloidal stability of warm clouds. *Tellus,* **10,** 256–271.
Srivastava, R. C., 1991: Growth of cloud drops by condensation: Effect of surface tension on the dispersion of cloud drop sizes. *J. Atmos. Sci.,* **48,** 1596–1605.
Telford, J. W., and S. K. Chai, 1980: A new aspect of condensation theory. *Pure Appl. Geophys.,* **118,** 720–742.
Tennekes, H., and J. L. Lumley, 1990: *A First Course in Turbulence.* The MIT Press, 300 pp.
Twomey, S., 1959: The nuclei of natural cloud formation. Part II: The supersaturation in natural clouds and the variation of cloud droplet concentration. *Pure Appl. Geophys.,* **43,** 243–249.
Warneck, P., 1988: *Chemistry of the Natural Atmosphere.* Academic Press, 757 pp
Warner, J., 1969a: The microstructure of cumulus cloud. Part I. General features of the droplet spectrum. *J. Atmos. Sci.,* **26,** 1049–1059.
——, 1969b: The microstructure of cumulus cloud. Part II. The effect on droplet size distribution of the cloud nucleus spectrum and updraft velocity. *J. Atmos. Sci.,* **26,** 1272–1282.
Willeke, K., and K. T. Whitby, 1975: Atmospheric aerosols: Size distribution interpretation. *J. Air Pollut. Control Assoc.,* **25,** 529–534.
Woodcock, A. H., 1950: Condensation nuclei and precipitation. *J. Meteor.,* **7,** 161–162.
——, 1952: Atmospheric salt particles and raindrops. *J. Meteor.,* **9,** 200–212.
Young, K. C., 1993: *Microphysical Processes in Clouds.* Oxford University Press, 427 pp.
——, and A. J. Warren, 1992: A reexamination of the deviation of the equilibrium supersaturation curve for soluble particles. *J. Atmos. Sci.,* **49,** 1138–1143.